On the competition between nucleation and thickening in deformation twinning of face-centered cubic metals

Matthew Daly,[a,b,*] Ashok Kumar[c], Chandra Veer Singh,[b,c] Glenn Hibbard[b]

[a]*Department of Civil and Materials Engineering, University of Illinois at Chicago – 842 W. Taylor St., 2095 ERF (MC 246), Chicago, IL, 60607, United States*

[b]*Department of Materials Science and Engineering, University of Toronto – 184 College St., Suite 140, Toronto, Ontario, M5S3E4, Canada*

[c]*Department of Mechanical and Industrial Engineering, University of Toronto – 5 King's College Rd., Toronto, Ontario, M5S3E4, Canada*

ABSTRACT

The process of deformation twinning significantly influences the flow behavior of metals through its signature features – plasticity accommodation *via* twinning shear and crystal segmentation from the creation of twin boundaries. While the competition between deformation twinning and dislocation slip can be understood from fundamental physical metallurgy parameters, the link between intrinsic material properties and the evolution of deformation twin microstructures has yet to emerge. Here, we report a general methodology to evaluate the competition between nucleation and thickening of deformation twins in face-centered cubic metals. Our approach leverages the critical energies of the generalized stacking fault landscape to simulate deformation twin evolution using the kinetic Monte Carlo method. Differences in twinning behaviors are found to be intimately related to the relevant deformation process barriers of each material. Inspired by the underlying deformation kinetics, an analytical model is developed to predict the evolution of deformation twin microstructures, which provides a scalable framework for investigations of crystal segmentation. From this model, a new criterion based on intrinsic material parameters is derived to distinguish between nucleation-favored and thickening-favored

[*]Corresponding author: mattdaly@uic.edu (M. Daly)

deformation twinning regimes. This criterion provides new understanding of twin evolution pathways, which operate as a sub-branch under the traditional categories of deformation twinning and dislocation slip. This analysis also finds direct applications in crystal plasticity models, where first-principles estimators for dynamic microstructure segmentation are beneficial to predictive accuracy and removing reliance on phenomenological observations.

Keywords: Deformation Twinning; Stacking fault energy; Monte Carlo simulation; Dynamic Hall-Petch effect; Strain hardening

---

1. INTRODUCTION

The mesoscale plastic behavior of face-centred cubic (FCC) metals is determined by the interplay of competing deformation mechanisms. Amongst these mechanisms, dislocation slip and deformation twinning are widely regarded as two of the most important dissipative processes. Indeed, the relative contributions of these mechanisms to overall plasticity offer fundamental insights into the connection between intrinsic material properties and emergent deformation behavior. Furthermore, an understanding of the competition between these mechanisms guides improvements to work hardening behavior and enables synergistic microstructure design. Recognition of these critical aspects within the metallurgy community has led to a number of seminal works seeking to provide a parameter-based predictor of mechanistic competition. For example, Tadmor and coworkers [1–3] used the generalized stacking fault (GSF) energy surface to develop a *twinnability* criterion, which quantifies the competition between slip and deformation twinning in proportion to the ratio of unstable stacking and twin fault energies. Other notable twinnability criteria based on the GSF energy landscape have been proposed by Asaro and Suresh [4], Jin *et al.* [5], and Jo *et al.* [6]. A comparative analysis of these criteria is discussed in a comprehensive review from De Cooman *et al.* [7]. A description of these twinnability criteria

highlighting the relevant GSF parameters is provided in Table 1. The specific deformation modes and associated twinnability criteria ranges are also provided. Schematic descriptions of the relevant GSF parameters in Table 1 are provided in Figure 1. While certainly insightful as a predictor of the relative competition between incipient deformation mechanisms, these criteria alone cannot capture the finer details of microstructure evolution, which ultimately underpins plasticity and hardening phenomena.

In comparison to slip, where dislocation glide results in the restoration of a perfect lattice, deformation twinning induces morphological changes in a microstructure that significantly influence mechanical behavior. More precisely, the nominal carriers of plasticity in deformation twinning (*i.e.*, Shockley partial dislocations) enable dynamic refinement of microstructure through the creation of intragranular planar faults (*i.e.*, stacking faults) that serve as strong barriers to dislocation glide during plastic loading. The activation of deformation twinning mechanisms therefore enables two key features: plasticity *via* twinning shear and crystal hardening. Indeed, the combined action of these deformation processes has been found to underpin exceptional performance in a varied range of FCC metallic systems. Perhaps one of the best known of these material families is the high manganese austenitic steels, also referred to as twinning-induced plasticity (TWIP) steels [8,9], which exhibit toughening behavior that overcomes traditional strength/ductility trade-offs. More recently, observation of the TWIP effect has been reported in iron-based high entropy alloy systems [10] – demonstrating the broader applicability of deformation twinning mechanisms. Beyond ferrous systems, Lu and coworkers have explored the mechanical behavior of nano-twinned copper [11–13]. Although the twins studied in this system are formed by electrodeposition-induced crystal growth processes, the influence of growth twin lamellae on work hardening in these structures is related to the hardening phenomena induced by

the planar faults created during mechanical twinning.

The growing interest in deformation twinning research within the metallurgy community has also given rise to a commensurate increase in theoretical modeling efforts. A common element in many such models is the inclusion of the signature features of deformation twinning: plastic accommodation and crystal hardening *via* dynamic grain refinement. Significant works are found in the dislocation storage models of Bouaziz and co-workers [14–17], where the influence of deformation twins on the flow behavior of TWIP steels is integrated directly into the traditional Kocks-Mecking work hardening approach [18]. In addition to these theories, deformation twinning phenomena have also been incorporated into the constitutive relations of crystal plasticity models. Important early contributions include works from Van Houtte [19] and Tomé *et al*. [20]. Kalidindi [21] employed a multiplicative decomposition of the deformation gradient to accommodate crystal reorientation from deformation twinning. Abdolvand *et al*. [22] incorporated Kalidindi's approach into the crystal plasticity finite element method. Additional refinements using explicit and homogenization-based methods have also been proposed by Ardeljan *et al*. [23] and Tadano *et al*. [24], respectively. Initially, crystal plasticity studies focused on low-symmetry hexagonal systems, where plasticity by deformation twinning is most common. For example, Salem *et al*. [25] applied the framework of Kalidindi to study strain hardening in α-titanium [25], and Beyerlein and Tomé [26] demonstrated a constitutive law for deformation twinning in zirconium. Recent studies have expanded the scope of deformation twinning crystal plasticity models to include FCC systems. For instance, reports from Shiekhelsouk *et al*. [27] and Sun *et al*. [28] provide micromechanical models to describe the flow behavior of TWIP steels, and a recent work from McCormack *et al*. [29] has added detwinning effects to the constitutive relations.

A critical element shared by these plasticity models is the treatment of crystal hardening under

deformation twinning. One common approach is to consider the deformation twin as a crystallographic barrier with static dimensions that occupies an overall volume defined by the evolution of the twinned material fraction [14–17,26,27,29]. Increases to the twinned material fraction are treated explicitly as the nucleation of new deformation twins with an assumed thickness. Hardening effects arise due to reductions in the dislocation mean free path created by these deformation twin barriers. The simplicity of this assumption belies the nature of deformation twinning, whereby both nucleation of new twins and thickening of existing twins are possible outcomes in response to increments in the deformation twin-accommodated plastic strain. Furthermore, this assumption inherently tethers these plasticity models to phenomenological theories of twin evolution, which are based on empirical inputs. This shortcoming in existing theories raises an interesting fundamental question: under which conditions do separate deformation twins nucleate or existing deformation twins thicken in response to plastic deformation? Nucleation-based deformation twinning causes a rapid segmentation of a microstructure and significant grain refinement, whereas deformation by twin thickening leads to a unit-step decrease in twin lamella spacing, as defined by the interplanar spacing of {111} slip planes. An intrinsic material tendency towards the former behavior has significant implications on the rate at which the mean free path between obstacles decays, and consequently, on hardening behavior. This question has been considered in the works of Ardeljan *et al*. [23] and Wang *et al*. [30] within the context of heterogeneities in stress field along twin-parent interfaces. However, an intrinsic material determination from the perspective of the GSF landscape is currently absent from the literature.

Here, we examine the intrinsic material properties that underpin the competition between nucleation and thickening in the deformation twinning of FCC metals. The relative competition

between these events is considered through kinetic Monte Carlo (kMC) simulations of common FCC metals, for which the GSF energies are well understood. Using the rate laws derived for kMC simulations, an analytical model and criterion is proposed to evaluate the kinetic competition between nucleation and thickening phenomena. The results of kMC studies and predictions from analytical modeling are validated using molecular dynamics (MD) simulations. The outcomes of this study are two-fold. In a fundamental sense, the proposed analytical model extends the twinnability criterion originally conceived by Tadmor and coworkers [1–3], by providing a generalized first-principles method to evaluate microstructure evolution under deformation twinning in FCC metals and alloys. Additionally, predictions based on analytical formulations can be implemented in crystal plasticity theories to incorporate the evolution of twin thicknesses and lamella spacing during deformation twinning, without the need for empirical fitting or phenomenological observations.

2. METHODOLOGY

2.1. Kinetic Monte Carlo Model

Kinetic Monte Carlo simulations of deformation twinning were performed using the methodology outlined in Bortz *et al*. [31] on five common FCC metals (Ag, Al, Cu, Ni, and Pb). These materials were selected to cover a wide range of GSF energies, including low and high stacking fault energy materials (*e.g.,* Ag and Al, respectively). Although materials such as Al and Ni do not exhibit pronounced deformation twinning, except in specific microstructures (*e.g.,* nanocrystalline Al [32,33]), they were selected in order to provide observation of a range of theoretical deformation twinning behaviors. A single crystal grain was assumed for all kMC simulations with orthogonal x and y axes directed along the $< 11\bar{2} >$ and $< 111 >$ crystal directions, respectively. This orientation was established to enable direct measurement of twin

spacing and thickness from a $< 1\bar{1}0 >$ zone axis. Simulation cells measured $M\vec{b}$ by Nd, where M and N are integers, $\vec{b}$ is the magnitude of the $< 11\bar{2} >$-type partial dislocation, and d is the spacing between $\{111\}$-type slip planes. The simulation cell is designed with free surfaces along the *x* axis and periodic boundaries along the *y* axis.

Two kinetic processes were considered in these simulations: partial dislocation nucleation and partial dislocation glide, which define deformation twin nucleation/thickening and the lateral growth of twin lamellae, respectively. Incipient formation of a deformation twin is considered as the nucleation and glide of a single Shockley partial dislocation across the simulation cell, forming an intrinsic stacking fault (ISF). Progressive nucleation and glide of Shockley partials on adjacent $\{111\}$ slip planes leads to the formation of a two-layer extrinsic stacking fault (ESF), and subsequently, thickening of a multi-layer twin fault (TF) that is bordered by coherent twin boundaries. Nucleation of deformation twins is achieved through a boundary/surface-mediated formation mechanism, as is common in observations of deformation twinning of FCC metals and alloys such as: nanowires [34], nano-sized thin film coatings [35], nanocrystals [36], and TWIP steels [9]. These nucleation events may be distinguished from pole-based deformation twin formation mechanisms [37]. Figure 1a provides a schematic of the simulation cell depicting the various planar fault morphologies that are formed by deformation twinning processes. All dislocations considered in this study were leading 90˚ edge-type Shockley partial dislocations. In order to obtain a direct assessment of the competition between twin nucleation and thickening, dislocation slip processes including the emission of trailing partials, dislocation cross-slip, and dislocation constrictions are not considered.

The kinetics of deformation twinning are examined through consideration of the relevant GSF energies. Figure 1b illustrates a typical section of the GSF energy (γ) landscape along the $< 11\bar{2} >$

crystal direction. The process barrier for the nucleation (E_1) and thickening (E_2, E_3 …, E_∞) of a deformation twin is defined here as the difference between the energy of the existing fault and the peak fault energy of the subsequent defect along the nucleation/growth pathway. The peak energies γ_{usf}^{1} and γ_{usf}^{2} refer to the unstable stacking fault energies overcome to form an ISF and ESF, respectively, and $\gamma_{utf}^{3} \cdots \gamma_{utf}^{\infty}$ indicate the unstable twin fault energies of an embryotic and thickened deformation twin, respectively. This notation for GSF energies used herein has been adapted from Jin *et al*. [5]. For each unstable energy, the superscript refers to the number of partial dislocations required to create the fault structure under activation. Values for the critical energies of the GSF landscape (*i.e.,* γ_{usf}^{1}, γ_{usf}^{2}, γ_{utf}^{∞}, γ_{isf}, γ_{esf}, and γ_{tf}) are obtained from first-principles density functional theory calculations as reported in Ref. [5]. The zero Kelvin energies are used as kinetic predictors herein, as is normal practice [7], given the lack of experimental measurement of the GSF landscape at finite temperature. The transition of thickening stages from incipient planar faults (i.e., ISFs and ESFs defined by $E_1$and E_2, respectively) to mature deformation twins is considered through examination of the GSF diagram. In FCC metals, the GSF energies are known to stabilize after formation of an ESF [38], which may be considered as a twin embryo with two proximate twin boundaries. Therefore, the process barrier for the formation of the twin embryo is calculated as: $E_3 = \gamma_{utf}^{3} - \gamma_{esf} \approx \gamma_{usf}^{2} - \gamma_{esf}$ and the energy of the twin embryo is $\approx 2\gamma_{tf}$, where γ_{tf} is the energy of an isolated twin boundary. The process barrier for deformation twin thickening (*i.e.,* growth beyond three layers) is assumed to be defined by E_∞, which has almost the same magnitude as E_3 for all materials considered in this study. These approximations for GSF energies are common within the community as discussed in De Cooman *et al.* [7].

The rates (R_i) of nucleation and glide events along the i^{th} slip plane in the kMC simulation cell are assumed to follow an Arrhenius relation and are described by the following expression:

$$R_i = R_o \exp\left\{\frac{-(\hat{\sigma}_i - \sigma_i)V}{k_b T}\right\} \quad (1)$$

where R_o is taken as the Debye frequency, T is the temperature (set at 300 K for all simulations), k_b is the Boltzmann constant, V is the activation volume (taken as $10\vec{b}^3$, see Ref. [39]), and σ_i and $\hat{\sigma}_i$ are the elastic shear and activation stresses operative at the deformation site on the i^{th} slip plane, respectively. At each step in the kMC model, $\hat{\sigma}_i$ is calculated based upon consideration of the deformation history. If a partial dislocation is not present on the i^{th} slip plane, then $\hat{\sigma}_i$ defines the barrier to dislocation nucleation. This barrier is calculated based on the existence and type of fault on adjacent slip planes (see Figure 1a). However, in the case that a dislocation is present, $\hat{\sigma}_i$ describes the barrier to dislocation glide (*i.e.,* the Peierls-Nabarro stress, σ_{PN}, see Figure 1a). According to the analysis of Ogata *et al.* [38], the relevant segments of the GSF energy curve represent a Peierls potential, which can be used directly to determine process barrier $\hat{\sigma}_i$ of partial dislocation nucleation. By contrast, if glide is operative, then $\hat{\sigma}_i$ is determined from solutions to the Peierls-Nabarro problem for a partial edge dislocation (*e.g.,* [40]). These considerations lead to a conditional definition of $\hat{\sigma}_i$ which follows as:

$$\hat{\sigma}_i = \begin{cases} \dfrac{\pi E_i}{\vec{b}}, twin\ nucleation/thickening \\ \dfrac{2G}{3(1-\nu)} exp\left\{\dfrac{-4\pi\varsigma}{3\vec{b}}\right\}, glide \end{cases} \quad (2)$$

where E_i is the process barrier of the corresponding fault structure in the deformation twin pathway, G is the shear modulus, ν is Poisson's ratio, and $\varsigma = \frac{G\vec{b}^2}{4\pi^2(1-\nu)E_i}$ is the half-width of the dislocation core. The mesoscale evolution of microstructure morphology is therefore determined by the interplay of two unique deformation processes, each with topology-sensitive process barriers. Table 2 provides the material parameters for all kMC simulations performed in this study. The barrier stress ($\hat{\sigma}_i$) can be lowered by the shear stress that exists at the relevant location along

each slip plane (*i.e.,* nucleation site or gliding dislocation). The shear stress (σ_i) applied at an activation site on plane i is calculated additively from elastic field contributions of partial edge dislocations that exist in the simulation cell. Individual dislocation shear stress fields are calculated using the Volterra approach [41], and summed to yield the total barrier reduction. Free surface effects are considered by modifying the Volterra solution to include image dislocations, which enforce vanishing shear stress fields along free surfaces (*i.e.,* the $< 11\bar{2} >$ surfaces in the simulation cell). In addition to internal stress fields, σ_i can also arise from external far-field loadings. Although far-field loadings can increase the rates of overall deformation, they are not expected to disproportionately bias nucleation or thickening kinetics due to an equal effect in lowering all process barriers and are not explicitly applied in kMC simulations. However, the formulation developed herein is sufficiently general to include the effects of far-field loads. Further details and equations used in elastic field calculations are provided in the Supplementary Material.

Implementation of Eqs. (1)-(2) with the kMC method for each active site in the simulation cell enables a kinetically-weighted observation of deformation twinning progression, where the likelihood of nucleation, thickening, and glide events are determined by the current cell configuration (as depicted in Figure 1a). The nucleation of twins is treated as a nominally homogeneous phenomenon, where heterogeneities arise from dislocations and fault structures from previous deformation steps. This may be distinguished from heterogeneous twin formation schemes (*e.g.*, as in Ref. [42]), which rely on specific pre-existing flaws. The simulation cells are initialized with no dislocations or twinned material present and simulations are terminated once the deformation twin fraction (F) reached 0.15. The selection of this termination criteria is based on the typical saturation values of deformation twin fractions, as discussed in a comparative analysis from De Cooman et al. [7]. At each timestep, F is measured from a lineal section of the

simulation cell, and the number of twins (N_T) across this section is recorded. In addition to the number of twins, the twin thicknesses (λ) and free paths (ρ) can also be calculated. Figure 2 provides a schematic of a simulation cell with these parameters featured. Although ISFs and ESFs are not explicitly considered as fully developed deformation twins, they are also included in parameter measurements as they also represent structures which segment the simulation cell and lead to dynamic grain refinement.

2.2. Analytical Model

The competition between nucleation and thickening of deformation twins may be analytically examined through consideration of the kinetics for the formation of new twins. The rate of change in the number of deformation twins in the simulation with respect to the change in the twinned material fraction $\left(\frac{dN_T}{dF}\right)$ is related to the probability of twin nucleation (P_N) by:

$$\frac{dN_T}{dF} = NP_N \tag{3}$$

Assuming all glide events have been exhausted, P_N is defined as the ratio of twin nucleation rates (R_N) to the total rates of all dislocation nucleation events (*i.e.*, the sum of twin nucleation and twin thickening (R_T) rates). From Eqs. (1)-(2):

$$P_N = \frac{R_N}{R_N + R_T} \tag{4a}$$

$$= \frac{\sum_{i=1}^{N-FN-2N_T} exp\left\{\frac{-V}{k_bT}\left(\frac{\pi E_1}{\vec{b}} - \sigma_i\right)\right\}}{\sum_{i=1}^{N-FN-2N_T} exp\left\{\frac{-V}{k_bT}\left(\frac{\pi E_1}{\vec{b}} - \sigma_i\right)\right\} + \sum_{j=1}^{2N_T} exp\left\{\frac{-V}{k_bT}\left(\frac{\pi E_j}{\vec{b}} - \sigma_j\right)\right\}} \tag{4b}$$

where the terms $N - FN - 2N_T$ and $2N_T$ represent the remaining slip planes available for twin nucleation and thickening at a fraction of F, respectively. Here, $2N_T$ represents the upper bound

for thickening sites as there are a number of twin configurations where sites are shared between proximate twins. Since dislocations were generally observed to glide a significant distance (typically across the cell) from the free surface before a subsequent nucleation event, the elastic stresses have been neglected. This assumption may introduce deviations in analytical predictions of nucleation probabilities for much larger systems, where the dislocation density may vary substantially from the current models. Yet, this assumption was found to be appropriate for all simulations considered herein. Furthermore, given that nominal process barriers for fault thickening events (*i.e.*, E_2, E_3 …, E_∞) are approximately equal, thickening of deformation twins is assumed to be reasonably represented by the E_∞ barrier. Application of these assumptions with Eqs. (3)-(4b) enables the formulation of the differential equation:

$$\frac{dN_T}{dF} - N\left\{\frac{(N - FN - 2N_T)exp\{-A\}}{(N - FN - 2N_T)exp\{-A\} + 2N_T exp\{-B\}}\right\} = 0 \tag{5}$$

where $A = \frac{V\pi E_1}{k_b T\vec{b}}$ and $B = \frac{V\pi E_\infty}{k_b T\vec{b}}$. Eq. (5) is readily solved using the 4th order Runge-Kutta numerical method. Additional parameters such as the average twin thickness ($\bar{\lambda}$) and the mean free path between twins ($\bar{\rho}$) can then be calculated from N_T as follows:

$$\bar{\lambda} = \frac{FD}{N_T} \tag{6a}$$

$$\bar{\rho} = \frac{(1 - F)D}{N_T} \tag{6b}$$

where $D = Nd$ is the crystal size, and the 'bar' indicates mean thickness and free path values, as opposed to the individual measurements depicted schematically in Figure 2. Under similar arguments to those presented in developing Eq. (5), we define here a *twin nucleation tendency* parameter (η), which describes the competition between nucleation and growth. This parameter is calculated as the ratio between the probability for twin nucleation and thickening using the

following relation:

$$\eta = \frac{R_N}{R_T} = \left(\frac{N - FN - 2N_T}{2N_T}\right) exp\left\{\frac{-V\pi}{k_b T\vec{b}}(E_1 - E_\infty)\right\} \quad (7a)$$

$$= \left(\frac{\bar{\lambda}(1-F)}{2F} - 1\right) exp\left\{\frac{-V\pi}{k_b T\vec{b}}(E_1 - E_\infty)\right\} \quad (7b)$$

Examination of Eqs. (7a) and (7b) provides interesting implications. Perhaps most notably, the model predicts that kinetic competition is directly proportional to the difference between process barriers required for fault nucleation ($E_1 = \gamma_{usf}^1$) and thickening ($E_\infty = \gamma_{utf}^\infty - \gamma_{tf}$). Collectively, the solutions to Eqs. (5)-(7b) provide an estimate for twin evolution kinetics in FCC metals using intrinsic material parameters and without the need for property fitting or phenomenological observations (*e.g.,* as in Refs. [14–16,43,44]) .

While the proposed kMC and analytical models provide insight into deformation twinning evolution and kinetics, it is important to consider the limitations on the applicability of these formulations. Indeed, in addition to the approximations undertaken when deriving the various formulae, the approach implemented in kMC simulations and analytical derivations undertakes two significant assumptions. Namely, deformation twinning is the only plasticity mechanism considered, and activation of nucleation sites is defined explicitly by the GSF energies. Competing deformation mechanisms such as dislocation slip, and the influence of microstructure on activation energies (*e.g.,* stress concentrators at crystal interfaces) are not currently considered. A more detailed discussion of these and additional model limitations and assumptions is provided in the Supplementary Material.

2.3. Molecular Dynamics Simulations

The assumptions undertaken in kMC and analytical modeling efforts motivate the search for an independent method to validate nucleation and thickening predictions. In this regard, the

deformation of a nanowire offers many parallels to the nucleation processes examined in the kMC simulations. Indeed, the free surfaces of a nanowire are known to serve as nucleation points for Shockley partial dislocations and nanowires are often reported to exhibit twin faulted structures after deformation [45]. Furthermore, a sufficiently long nanowire possesses enough nucleation points such that a large sampling of sites with near equal barriers are available simultaneously for activation. The kinetics of Shockley partial nucleation in nanowire deformation are therefore anticipated to be representative of the processes studied in the kMC model.

Deformation processes in nanowires are studied herein using MD simulations. The implementation of MD simulations for this purpose offers several advantages. Namely, the size and timescale limitations that typically restrict the applicability of MD predictions are, in the case of this study, of distinct benefit. For instance, the thickness of nanowires is typically smaller than the equilibrium dislocation dissociation width of most FCC metals examined in this study, which enables the propagation of continuous fault structures across the entire nanowire cross-section. Furthermore, the extremely high strain rates implemented in MD simulations lead to the development of large stresses due to reduced thermal activation of low-stress, quasi-static dissipative processes. In this regard, sufficient stress is sustained in the nanowire cross-section such that surface nucleation of Shockley partials manifests as the dominant plasticity mechanism. In other words, the typically limiting restrictions of MD simulations are leveraged here to probe the specific deformation pathway explored in kMC calculations. This approach is inspired, in part, by the work of Yu *et al*. [46] on deformation twinning in magnesium nanowires.

MD simulations of nanowire deformation were performed using the Large-scale Atomic/Molecular Massively Parallel Simulator (LAMMPS) [47]. The Open Visualization Tool [48] was used to visualize atomic topologies in MD simulations and twinning fault structures were

identified using the Crystal Analysis Tool [49]. Interatomic interactions were modeled using a screened set of freely available potentials. Given the sensitivity of model predictions to fault energies, it is critical that MD potentials capture the essential energies of the GSF surface. For this purpose, several popular interatomic potentials were evaluated to assess their correspondence with the first-principles-based energies reported in Ref. [5]. From this screening process, suitable potentials were identified for Ag [50], Cu [51], and Al [52]. Further details of the MD simulations and the interatomic potential screening process are provided in the Supplementary Material.

3. RESULTS AND DISCUSSION

The kMC model presented in Section 2 has been implemented to study two separate system configurations: a *square* simulation cell and a *nanowire* cell. All square simulation cells measure $300\vec{b}$ by $300d$ and are used in studies of Ag, Al, Cu, Ni, and Pb. Each square simulation study is replicated 100 times for statistical sampling. The dimensions of the nanowire kMC studies are varied to match the sizes of MD simulation cells and were comparably smaller. Each nanowire simulation study is replicated 500 times for statistical sampling and results are reported for Ag, Cu, and Al, which are the systems examined in MD calculations. In both the square and nanowire studies, results from kMC simulations were found to converge well below the replication limit. A sensitivity analysis of the square cell is provided in the Supplementary Material. The purpose of this subdivision of studies is to assess the predictive capabilities of the derived analytical model in kMC simulations with a shared size (square cell) and then validate both the kMC and analytical models using MD simulations (nanowire cell). All error bars are reported as ± 1 standard deviation.

3.1. Evolution of Deformation Twinning Morphologies (Square Cell)

Figure 3 presents typical snapshots of the kMC simulation cell at different stages of deformation twinning in Ag and Al. The colored regions represent areas which have undergone twinning. As shown in the figure, deformation twinning proceeds with the nucleation and

thickening of twins *via* the glide of partial dislocations across the simulated crystal. A clear distinction between the behaviors of Ag and Al is apparent with the former nucleating several thin deformation twins and the latter developing one thick deformation twin. These morphologies are qualitatively supported by the experimental reports. For example, Ramachandramoorthy *et al*. [53] observed a distributed formation of thin twin lamellae (on the order of < 5d thick) in *in situ* high resolution transmission microscopy (HRTEM) tensile studies of single crystal Ag nanowires. Whereas, Li *et al.* [54] observed thickening of a single twin during *in situ* straining of single crystal Al foils under HRTEM observation. Although the Li *et al*. study uses a crack-tip to stimulate deformation twinning, the post-nucleation thickening of the twin embryo grows outside of the sharp notch. The preference for continued growth, as opposed to a new twin nucleation event, highlights the distinct role that intrinsic material properties hold in determining deformation twin evolution. Snapshots of deformation twinning in the other materials studied as well as videos of the evolution of deformation twins are available as Supplementary Material.

The evolution of the average twin density of deformation twins (n_T) is plotted in Figure 4 for each material examined in this study. The twin density of deformation twins is calculated here as a number density from the ratio of the number of twins to the cell length (*i.e.,* $n_T = N_T/Nd$). For all materials a monotonic increase in the twin density is observed with Ag and Ni/Al showing the largest and smallest values of n_T respectively. While materials such as Ag and Cu exhibited a tendency to nucleate several twins during kMC simulations, deformation in Ni and Al was limited to thickening of a single twin. The small differences in the number densities of Al and Ni reflect the changes in simulation cell length arising from their differing lattice constants. Examination of Figure 4 shows an excellent agreement between the kMC data and the predictions of the analytical model (*i.e.,* the numerical solution of Eq. (5)). Consequently, the analytical model can be used as

a direct method to predict competition between nucleation and thickening behaviors in deformation twinning. Moreover, the geometric and material inputs required for the model are readily accessible in the literature or directly through first principles calculations. In addition to the twin number density, the kMC model can be used to predict other complementary twinning evolution parameters such as the average twin thickness (*i.e.,* $\bar{\lambda}$) and mean free path (*i.e.,* $\bar{\rho}$). Analytical estimates can be obtained for these parameters by transforming calculations of n_T using Eqs. (6a) and (6b). Predictions for the evolution of $\bar{\lambda}$ using the kMC model and analytical framework are provided in Figure 5. As shown in the figure, materials such as Ag and Cu exhibit only marginal thickening, which is expected from the twin number density data. Whereas, Ni and Al exhibit a linear thickening over the range of twin fractions studied. The diverse thickening behaviors revealed by these calculations underscore the oversimplified treatment of deformation twinning in current plasticity theories, where the twinning faults are treated as obstacles with static dimensions. Indeed, the analytical model presented herein finds direct applications in the plasticity theories of Bouaziz and coworkers [14–17], Shiekhelsouk *et al*. [27], and McCormack *et al*. [29], where hardening behaviors exhibit a strong sensitivity to fitting of twin thicknesses. More broadly, this approach could also be applied to deformation twinning models of hexagonal systems, as in Beyerlein and Tomé [26]. Predictions for evolution of $\bar{\rho}$ are complementary to the average twin thickness and are included in the Supplementary Material.

Figure 6 presents the evolution of the twin nucleation tendency parameter as a function of twin fraction for each FCC metal. Both kMC simulation results and analytical predictions are plotted, showing excellent agreement. As anticipated from the twin densities reported in Figure 4, Ag and Cu possessed the highest tendencies for twin nucleation, reaching ratios as high as ≈ 42 and 12, respectively, during the initial stages of deformation. Conversely, Ni and Al exhibited a strong

preference for twin thickening, with η measuring in the range of ≈ 1 – 1.7x10^{-3}. In general, the analytical model is able to capture the kMC results well within the margins of statistical scatter. It should be noted that the error for the initial datapoint of each material is effectively zero as the outcome of the first kinetic event in the kMC simulation is deterministic (*i.e.,* event must be ISF nucleation). Additionally, error bars increase abruptly for some materials (*e.g.*, Ni and Al) when a small number of simulations diverged from the most probable outcome (*i.e.*, a single twin segmenting the simulation cell). As the twin number density is calculated as an integral parameter, the divergence of some simulation replications manifests as abrupt changes in the error bar magnitude. For other materials (*e.g.*, Ag, Pb, and Cu), where differing numbers of twins are commonly observed at all stages of deformation, error bars appear continuously.

3.2. Validation of kMC and Analytical Models (Nanowire Cell)

Although the excellent agreement between kMC simulations and the analytical model predictions are encouraging, these estimators for deformation twinning competition are fundamentally rooted in similar assumptions. In this regard, MD simulations serve as an independent predictor of deformation twinning evolution, which may be compared against kMC and analytical predictions. For further specifics on the MD methodology, please see Section 2.3 and the Supplementary Material. Figure 7 presents snapshots for MD tensile simulations of each material at $F \approx 0.15$. As intended, deformation twinning appears as a plasticity mechanism in the nanowire simulations. Several twinning fault structures are visible, including ISFs and TFs. ESFs are drawn here as TFs since the crystal analysis algorithm cannot currently distinguish between these structures. In Ag and Cu, deformation twinning was observed to be the dominant plasticity mechanism, whereas a mixture of slip and twinning were observed in Al nanowires, which is a result of its higher stacking fault energy. Nonetheless, the resulting deformation twin morphology in the Al nanowire can be compared to kMC results. Examination of the deformation twins in

Figure 7 shows qualitative agreement with the findings of the kMC simulations, where the Ag nanowire is segmented by a number of twinning faults and the Al nanowire exhibits only a single thickened twin.

In order to provide a quantitative comparison, complementary kMC simulations and analytical calculations were performed on cells matching the dimensions of the MD nanowire topologies. The agreement between kMC simulations and analytical calculations was again found to be excellent, highlighting the generality of these approach across different system configurations. A plot of the kMC and analytical predictions for twin density evolution in the nanowire cell is provided in the Supplementary Material. Figure 8 presents a comparison of twin density evolution in MD simulations and analytical calculations for the nanowire cell. In order to calculate the twin density and twin fraction from the MD snapshots an image processing algorithm was developed. Details of this algorithm are provided in the Supplementary Material. All five replications of the MD simulation data are plotted for each material (Ag, Cu, and Al) on the same plot. As shown in the figure, the analytical predictions are in excellent agreement with the MD data, which serves as a strong validation of the combined kMC/analytical approach developed in this study. The only noticeable deviations in predictions are found in the Al nanowire data presented in Figure 8c. These deviations (indicated by a star) are outliers that are the result of isolated instances of dislocation slip during nanowire deformation, which led to a temporary measurement artifact in the twin density. Glide of extended dislocations through the nanowire eliminated these outliers upon annihilation at the opposing free surface.

3.3. Size Effects and Scalability

The previous two systems examined in this study are restricted to nanoscale cell sizes. This restriction is due to computational limitations placed on kMC and MD simulations, which present feasibility issues for calculations on larger systems. In this section, the scalability of the analytical

model is examined. Careful examination of the twin number densities measured for the square (Figure 4) and nanowire (Figure 8) systems shows that there is a size effect in predictions. This size effect is expected to be the most pronounced in Al and Ni, which exhibit the least tendency to nucleate deformation twins. However, given a sufficiently large crystal the probability of nucleation will rise to compete with thickening events due to an increase in the available activation sites. This behavior is subject to saturation, where the twin density of these materials becomes decoupled from crystal size. While these crystal sizes are inaccessible using kMC or MD calculations, they can be explored through the derived analytical model. Figure 9 presents twin density calculations for Ag and Al for crystal sizes varying from 5 to 1000 nm. As indicated in the figure, the twin density converges at small crystal sizes (*i.e.,* $D > 10$ nm) for Ag, whereas Al twinning densities do not stabilize until crystals reach above 500 nm. Consequently, these findings place a threshold on the representative crystal sizes required to make size-independent predictions for twin number densities. For small crystal sizes (*e.g.,* $D = 5$ nm), the data does not extend to the plot origin. This is a result of the discrete increments in F that are more apparent in systems comprised of very few slip planes. Crystal size sensitivity calculations have been also performed for Cu, Pb, and Ni and are available in the Supplementary Material.

In addition to the twin number density, the nucleation tendency parameter also exhibits a size effect. Figure 10 presents surface plots of the twin nucleation tendency with respect to twin fraction and crystal size for Ag and Al. As shown in the figure, the evolution of the nucleation tendency of Al with twinning fraction is very sensitive to changes in crystal size, whereas Ag exhibits a comparatively moderate sensitivity to these parameters. However, η is maximized for both materials at low twin fractions, and progressively shrinks as more sites become available for thickening at increased F. The nucleation tendency behaviors of these materials are consistent with

the twin density results. Namely, the twin density of Ag saturates at very low crystal sizes whereas Al exhibits a significant size effect. Similar plots for Cu, Pb, and Ni are available in the Supplementary Material.

3.4. Criterion for Twin Nucleation Tendency

The generality of the analytical model developed herein motivates a critical examination of the relations between material parameters underpinning its predictions. In this regard, fundamental insight into the competition between nucleation and thickening kinetics in deformation twinning processes can be elucidated from careful examination of the constitutive equations. For example, the twin nucleation tendency (Eq. (7a)) is shown to depend on a combination of microstructure (*N*, *F*, and N_T), thermodynamic (*T*), and material parameters (*V,* $\vec{b}$, E_1, and E_∞). In relation to the GSF energies, η exhibits an exponential dependency on the difference of E_1 and E_∞. This insight is intuitive, as the twin nucleation tendency is expected to be sensitive to the difference between the barrier for twin nucleation ($E_1 = \gamma_{usf}^1$) and twin growth ($E_\infty = \gamma_{utf}^\infty - \gamma_{tf}$). Figure 11 presents the twin nucleation tendency parameter as a function of twin fraction and process barrier difference ($\Delta E_{1\infty} = E_1 - E_\infty$) for each material with an assumed crystal size of *D* = 1 μm. As shown in the figure, the twin nucleation tendency is found to be inversely proportional to the process barrier difference. Ag possesses the lowest $\Delta E_{1\infty}$ and exhibits the highest η, as the barriers for nucleation and thickening of deformation twins are nearly equivalent. On the other extreme, Ni shows the highest values of $\Delta E_{1\infty}$and lowest twinning tendency. These trends in η are found to be constant across all twin fractions.

A significant implication of this finding is that the process barrier can be utilized to develop a predictor for the competition between nucleation and thickening processes in deformation twinning. By setting the twin nucleation tendency to parity (*i.e.,* $\eta = 1$), the *twin nucleation*

tendency criterion (T_η) is derived from Eq. (7a) as follows:

$$T_\eta = \alpha - \beta \Delta E_{1\infty} \tag{8}$$

where $\alpha = ln\left(\frac{N-FN-2N_T}{2N_T}\right)$ and $\beta = \frac{V\pi}{k_b T \vec{b}}$. Under this description, nucleation of deformation twins is kinetically favored when $T_\eta > 0$ and thickening of existing twins is more likely when $T_\eta < 0$. The term α contains microstructure information regarding the system under consideration and $\beta \Delta E_{1\infty}$ holds the thermodynamic and material parameters. The distinction between nucleation and twinning may therefore be considered as a competition between available nucleation sites (α) and material-specific defect preferences ($\Delta E_{1\infty}$). Phrased differently, if a substance exhibits no preference for nucleation or twinning in its material constants (*i.e.,* $\Delta E_{1\infty} = 0$), then the likelihood for nucleation or thickening of deformation twins is purely a function of microstructure topology. Figure 12 plots the twin nucleation tendency criterion for each material at a crystal size of D = 1 μm. Examination of the figure data reveals nucleation-favored deformation in Ag and Cu, and thickening-favored twinning in Pb, Al, and Ni. Both Ag and Cu experience a gradual decrease in nucleation-favored deformation, reaching parity with thickening-favored twinning at twin fractions of ≈ 0.14 and 0.06, respectively. Although the connection between T_η and η is intuitive, given their shared derivation, the predictive relationship is non-trivial, as it cannot be replicated by existing metrics. Table 3 lists the twin nucleation tendency criterion after nucleation of the first ISF (η_1) for the data presented in Figure 12. These values are compared against the twinnability criteria of Tadmor and Bernstein [2], Asaro and Suresh [4], Jin *et al.* [5], and Jo *et al.* [6] (see Table 1 for a description of these parameters). As shown in the Table 3, T_η is the only parameter exhibiting a monotonic relationship with η_1, highlighting its utility as a predictor of nucleation and thickening-dominated behaviors. We should note that the referenced parameters were not explicitly formulated to distinguish between these competitive processes. However, a comparison is merited

to demonstrate the uniqueness of our criterion. Indeed, the predictive capabilities of T_η are perhaps the most significant outcome of this study. Through the development of this criterion, we have demonstrated a method to predict the morphology of deformation twins based on microstructural and first-principles inputs. In a broad sense, the twin nucleation tendency criterion developed here is a natural extension of the twinnability concept – adding a new branch to the deformation mechanism pathways that underpin microstructure evolution.

4. CONCLUSIONS

The competition between nucleation and thickening of deformation twins has been studied for five FCC metals (Ag, Cu, Pb, Al and Ni). For this purpose, a generalized simulation methodology based on the kMC method has been developed to study the twin number density evolution in nanoscale FCC systems. Results of kMC simulations indicate that Ag and Cu demonstrate nucleation-favored deformation (*i.e.,* high twin number densities), whereas Pb, Al, and Ni favor thickening of deformation twins (*i.e.,* low twin number densities). These results find direct applications in crystal plasticity theories, which currently ignore the dynamic growth processes of deformation twins and their role in crystal segmentation. Based on kMC results, a twin nucleation tendency parameter was developed to quantify the comparative kinetics of twin nucleation and thickening. The twinning evolution predictions from kMC calculations were further validated using direct MD simulations on comparable systems. A direct analytical framework was also derived from elements of the kMC method and was found to have excellent agreement with kMC and MD datasets. The critical features of this analytical framework rely on intrinsic material properties, and therefore, remove many elements of empirical fitting and phenomenological modeling from predictions. A notable outcome from analytical modeling was the demonstration of a crystal size effect, where results for thickening-dominated materials (*e.g.,* Pb, Al and Ni)

converged at larger crystal sizes as compared to nucleation-dominated systems (*e.g.,* Ag and Cu). The development of this analytical model also provides scalability to this approach, which overcomes the computational limitations of the kMC and MD methodologies – enabling access to crystal sizes beyond the nanoscale.

The results of this analysis provide key insights into the nature of deformation twinning in FCC metals. Trends in nucleation-favored and thickening-favored deformation were observed to be underpinned by intrinsic material parameters – namely, the critical energies of the GSF landscape. These trends in deformation preferences could not be rationalized using existing predictors in the literature. Therefore, a new criterion for the competitive processes of deformation twinning was developed from the GSF energies. This twin nucleation tendency criterion is explicitly formulated to differentiate between nucleation-favored and thickening-favored deformation twinning through consideration of microstructural and material parameters. In this regard, this criterion provides a focused understanding of twinning evolution pathways that operate as a sub-branch under the umbrella of the traditional FCC mechanisms of deformation twinning and dislocation slip.

ACKNOWLEDGEMENTS

This work was supported by the Natural Sciences and Engineering Research Council of Canada (NSERC) under the Discovery Grants Program (RGPIN-2018-04642); the University of Illinois at Chicago; and the University of Toronto. M. D. was supported by a Postgraduate Scholarship from NSERC (6799-425095-2012). C. V. S. was supported by an Early Research Award from the Ontario Ministry of Research, Innovation and Science (ER15-11-015). Computations were performed on the GPC supercomputer at the SciNet HPC Consortium [55]. SciNet is funded by: the Canada Foundation for Innovation; the Government of Ontario; Ontario Research Fund - Research Excellence; and the University of Toronto. This research was enabled in part by support provided by the Scinet HPC Consortium and Compute Canada (www.computecanada.ca). M. D.

would like to thank Professor Craig Foster for helpful discussions.

AUTHOR CONTRIBUTIONS

M. D. developed the kMC approach, analytical model, and molecular dynamics simulations with technical guidance from C. V. S. and G. H. Molecular dynamics simulations were performed by A. K. under guidance from M. D. The manuscript was written by M. D. with contributions from all other authors.

SUPPLEMENTARY MATERIAL

Supplementary Material is available online from the publisher or by request from the corresponding author (mattdaly@uic.edu).

COMPETING INTERESTS

The authors declare no competing interests.

REFERENCES

[1] E.B. Tadmor, S. Hai, A Peierls criterion for the onset of deformation twinning at a crack tip, J. Mech. Phys. Solids. 51 (2003) 765–793. doi:10.1016/S0022-5096(03)00005-X.

[2] E.B. Tadmor, N. Bernstein, A first-principles measure for the twinnability of FCC metals, J. Mech. Phys. Solids. 52 (2004) 2507–2519. doi:10.1016/j.jmps.2004.05.002.

[3] N. Bernstein, E. Tadmor, Tight-binding calculations of stacking energies and twinnability in fcc metals, Phys. Rev. B. 69 (2004) 094116. doi:10.1103/PhysRevB.69.094116.

[4] R.J. Asaro, S. Suresh, Mechanistic models for the activation volume and rate sensitivity in metals with nanocrystalline grains and nano-scale twins, Acta Mater. 53 (2005) 3369–3382. doi:10.1016/j.actamat.2005.03.047.

[5] Z.H. Jin, S.T. Dunham, H. Gleiter, H. Hahn, P. Gumbsch, A universal scaling of planar fault energy barriers in face-centered cubic metals, Scr. Mater. 64 (2011) 605–608. doi:10.1016/j.scriptamat.2010.11.033.

[6] M. Jo, Y.M. Koo, B.-J. Lee, B. Johansson, L. Vitos, S.K. Kwon, Theory for plasticity of face-centered cubic metals, Proc. Natl. Acad. Sci. 111 (2014) 6560–6565. doi:10.1073/pnas.1400786111.

[7] B.C. De Cooman, Y. Estrin, S.K. Kim, Twinning-induced plasticity (TWIP) steels, Acta Mater. 142 (2018) 283–362. doi:10.1016/j.actamat.2017.06.046.

[8] O. Grässel, L. Krüger, G. Frommeyer, L.W. Meyer, High strength Fe-Mn-(Al, Si) TRIP/TWIP steels development - properties - application, Int. J. Plast. 16 (2000) 1391–1409. doi:10.1016/S0749-6419(00)00015-2.

[9] I. Gutierrez-Urrutia, S. Zaefferer, D. Raabe, The effect of grain size and grain orientation on deformation twinning in a Fe-22wt.% Mn-0.6wt.% C TWIP steel, Mater. Sci. Eng. A. 527 (2010) 3552–3560. doi:10.1016/j.msea.2010.02.041.

[10] Y. Deng, C.C. Tasan, K.G. Pradeep, H. Springer, A. Kostka, D. Raabe, Design of a twinning-induced plasticity high entropy alloy, Acta Mater. 94 (2015) 124–133. doi:10.1016/j.actamat.2015.04.014.

[11] L. Lu, Y. Shen, X. Chen, L. Qian, K. Lu, Ultrahigh Strength and High Electrical Conductivity in Copper, Science (80-.). 304 (2004) 422–426. doi:10.1126/science.1092905.

[12] Y.F. Shen, L. Lu, Q.H. Lu, Z.H. Jin, K. Lu, Tensile properties of copper with nano-scale twins, Scr. Mater. 52 (2005) 989–994. doi:10.1016/j.scriptamat.2005.01.033.

[13] K. Lu, L. Lu, S. Suresh, Strengthening Materials by Engineering Coherent Internal Boundaries at the Nanoscale, Science (80-.). 324 (2009) 349–352. doi:10.1126/science.1159610.

[14] O. Bouaziz, N. Guelton, Modelling of TWIP effect on work-hardening, Mater. Sci. Eng.

A. 319–321 (2001) 246–249. doi:10.1016/S0921-5093(00)02019-0.

[15] S. Allain, J.-P. Chateau, O. Bouaziz, A physical model of the twinning-induced plasticity effect in a high manganese austenitic steel, Mater. Sci. Eng. A. 387–389 (2004) 143–147. doi:10.1016/j.msea.2004.01.060.

[16] O. Bouaziz, S. Allain, C. Scott, Effect of grain and twin boundaries on the hardening mechanisms of twinning-induced plasticity steels, Scr. Mater. 58 (2008) 484–487. doi:10.1016/j.scriptamat.2007.10.050.

[17] O. Bouaziz, Strain-hardening of twinning-induced plasticity steels, Scr. Mater. 66 (2012) 982–985. doi:10.1016/j.scriptamat.2011.11.029.

[18] U.F. Kocks, H. Mecking, Physics and phenomenology of strain hardening: the FCC case, Prog. Mater. Sci. 48 (2003) 171–273. doi:10.1016/S0079-6425(02)00003-8.

[19] P.V. Houtte, Simulation of the rolling and shear texture of brass by the Taylor theory adapted for mechanical twinning, Acta Metall. 26 (1978) 591–604. doi:10.1016/0001-6160(78)90111-6.

[20] C.N. Tomé, R.A. Lebensohn, U.F. Kocks, A model for texture development dominated by deformation twinning: Application to zirconium alloys, Acta Metall. Mater. 39 (1991) 2667–2680. doi:10.1016/0956-7151(91)90083-D.

[21] S.R. Kalidindi, Incorporation of Deformation Twinning in Models, Int. J. Plast. 46 (1998) 267–290.

[22] H. Abdolvand, M.R. Daymond, C. Mareau, Incorporation of twinning into a crystal plasticity finite element model: Evolution of lattice strains and texture in Zircaloy-2, Int. J. Plast. 27 (2011) 1721–1738. doi:10.1016/j.ijplas.2011.04.005.

[23] M. Ardeljan, R.J. McCabe, I.J. Beyerlein, M. Knezevic, Explicit incorporation of

deformation twins into crystal plasticity finite element models, Comput. Methods Appl. Mech. Eng. 295 (2015) 396–413. doi:10.1016/j.cma.2015.07.003.

[24] Y. Tadano, Y. Yoshihara, S. Hagihara, A crystal plasticity modeling considering volume fraction of deformation twinning, Int. J. Plast. 84 (2015) 88–101. doi:10.1016/j.ijplas.2016.05.002.

[25] A.A. Salem, S.R. Kalidindi, S.L. Semiatin, Strain hardening due to deformation twinning in α-titanium: Constitutive relations and crystal-plasticity modeling, Acta Mater. 53 (2005) 3495–3502. doi:10.1016/j.actamat.2005.04.014.

[26] I.J. Beyerlein, C.N. Tomé, A dislocation-based constitutive law for pure Zr including temperature effects, Int. J. Plast. 24 (2008) 867–895. doi:10.1016/j.ijplas.2007.07.017.

[27] M.N. Shiekhelsouk, V. Favier, K. Inal, M. Cherkaoui, Modelling the behaviour of polycrystalline austenitic steel with twinning-induced plasticity effect, Int. J. Plast. 25 (2009) 105–133. doi:10.1016/j.ijplas.2007.11.004.

[28] C.Y. Sun, N. Guo, M.W. Fu, S.W. Wang, Modeling of slip, twinning and transformation induced plastic deformation for TWIP steel based on crystal plasticity, Int. J. Plast. 76 (2016) 186–212. doi:10.1016/j.ijplas.2015.08.003.

[29] S.J. McCormack, W. Wen, E. V. Pereloma, C.N. Tomé, A.A. Gazder, A.A. Saleh, On the first direct observation of de-twinning in a twinning-induced plasticity steel, Acta Mater. 156 (2018) 172–182. doi:10.1016/j.actamat.2018.06.029.

[30] H. Wang, P.D. Wu, J. Wang, C.N. Tomé, A crystal plasticity model for hexagonal close packed (HCP) crystals including twinning and de-twinning mechanisms, Int. J. Plast. 49 (2013) 36–52. doi:10.1016/j.ijplas.2013.02.016.

[31] A.B. Bortz, M.H. Kalos, J.L. Lebowitz, A new algorithm for Monte Carlo simulation of

Ising spin systems, J. Comput. Phys. 17 (1975) 10–18. doi:10.1016/0021-9991(75)90060-1.

[32] X.Z. Liao, F. Zhou, E.J. Lavernia, D.W. He, Y.T. Zhu, Deformation twins in nanocrystalline Al, Appl. Phys. Lett. 83 (2003) 5062–5064. doi:10.1063/1.1633975.

[33] M. Chen, E. Ma, K.J. Hemker, H. Sheng, Y. Wang, X. Cheng, Deformation Twinning in Nanocrystalline Aluminum, Science (80-.). 300 (2003) 1275–1277. doi:10.1126/science.1083727.

[34] S. Lee, J. Im, Y. Yoo, E. Bitzek, D. Kiener, G. Richter, B. Kim, S.H. Oh, Reversible cyclic deformation mechanism of gold nanowires by twinning–detwinning transition evidenced from in situ TEM, Nat. Commun. 5 (2014) 3033. doi:10.1038/ncomms4033.

[35] S.H. Oh, M. Legros, D. Kiener, P. Gruber, G. Dehm, In situ TEM straining of single crystal Au films on polyimide: Change of deformation mechanisms at the nanoscale, Acta Mater. 55 (2007) 5558–5571. doi:10.1016/j.actamat.2007.06.015.

[36] Y.T. Zhu, X.Z. Liao, X.L. Wu, Deformation twinning in nanocrystalline materials, Prog. Mater. Sci. 57 (2012) 1–62. doi:10.1016/j.pmatsci.2011.05.001.

[37] J.A. Venables, Deformation twinning in face-centred cubic metals, Philos. Mag. 6 (1961) 379–396. doi:10.1080/14786436108235892.

[38] S. Ogata, J. Li, S. Yip, Energy landscape of deformation twinning in bcc and fcc metals, Phys. Rev. B. 71 (2005) 224102. doi:10.1103/PhysRevB.71.224102.

[39] R. Ramachandramoorthy, W. Gao, R. Bernal, H. Espinosa, High Strain Rate Tensile Testing of Silver Nanowires: Rate-Dependent Brittle-to-Ductile Transition, Nano Lett. 16 (2016) 255–263. doi:10.1021/acs.nanolett.5b03630.

[40] B. Joós, M.S. Duesbery, The Peierls Stress of Dislocations: An Analytic Formula, Phys.

Rev. Lett. 78 (1997) 266–269. doi:10.1103/PhysRevLett.78.266.

[41] J. Hirth, J. Lothe, Theory of dislocations, 1982.

[42] S. Kibey, J.B. Liu, D.D. Johnson, H. Sehitoglu, Predicting twinning stress in fcc metals: Linking twin-energy pathways to twin nucleation, Acta Mater. 55 (2007) 6843–6851. doi:10.1016/j.actamat.2007.08.042.

[43] L. Remy, Kinetics of f.c.c. deformation twinning and its relationship to stress-strain behaviour, Acta Metall. 26 (1978) 443–451. doi:10.1016/0001-6160(78)90170-0.

[44] J. Gil Sevillano, An alternative model for the strain hardening of FCC alloys that twin, validated for twinning-induced plasticity steel, Scr. Mater. 60 (2009) 336–339. doi:10.1016/j.scriptamat.2008.10.035.

[45] H.S. Park, K. Gall, J.A. Zimmerman, Deformation of FCC nanowires by twinning and slip, J. Mech. Phys. Solids. 54 (2006) 1862–1881. doi:10.1016/j.jmps.2006.03.006.

[46] Q. Yu, L. Qi, K. Chen, R.K. Mishra, J. Li, A.M. Minor, The nanostructured origin of deformation twinning, Nano Lett. 12 (2012) 887–892. doi:10.1021/nl203937t.

[47] S. Plimpton, Fast Parallel Algorithms for Short-Range Molecular Dynamics, J. Comput. Phys. 117 (1995) 1–19. doi:10.1006/jcph.1995.1039.

[48] A. Stukowski, Visualization and analysis of atomistic simulation data with OVITO–the Open Visualization Tool, Model. Simul. Mater. Sci. Eng. 18 (2010) 015012. doi:10.1088/0965-0393/18/1/015012.

[49] A. Stukowski, Structure identification methods for atomistic simulations of crystalline materials, Model. Simul. Mater. Sci. Eng. 20 (2012) 045021. doi:10.1088/0965-0393/20/4/045021.

[50] X.W. Zhou, R.A. Johnson, H.N.G. Wadley, Misfit-energy-increasing dislocations in vapor-

deposited CoFe/NiFe multilayers, Phys. Rev. B. 69 (2004) 144113. doi:10.1103/PhysRevB.69.144113.

[51] Y. Mishin, M.J. Mehl, D.A. Papaconstantopoulos, A.F. Voter, J.D. Kress, Structural stability and lattice defects in copper: Ab initio , tight-binding, and embedded-atom calculations, Phys. Rev. B. 63 (2001) 224106. doi:10.1103/PhysRevB.63.224106.

[52] R.R. Zope, Y. Mishin, Interatomic potentials for atomistic simulations of the Ti-Al system, Phys. Rev. B. 68 (2003) 024102. doi:10.1103/PhysRevB.68.024102.

[53] R. Ramachandramoorthy, Y. Wang, A. Aghaei, G. Richter, W. Cai, H.D. Espinosa, Reliability of Single Crystal Silver Nanowire-Based Systems: Stress Assisted Instabilities, ACS Nano. 11 (2017) 4768–4776. doi:10.1021/acsnano.7b01075.

[54] B.Q. Li, M.L. Sui, B. Li, E. Ma, S.X. Mao, Reversible Twinning in Pure Aluminum, Phys. Rev. Lett. 102 (2009) 205504. doi:10.1103/PhysRevLett.102.205504.

[55] C. Loken, D. Gruner, L. Groer, R. Peltier, N. Bunn, M. Craig, T. Henriques, J. Dempsey, C.-H. Yu, J. Chen, L.J. Dursi, J. Chong, S. Northrup, J. Pinto, N. Knecht, R. Van Zon, SciNet: Lessons Learned from Building a Power-efficient Top-20 System and Data Centre, J. Phys. Conf. Ser. 256 (2010) 012026. doi:10.1088/1742-6596/256/1/012026.

[56] H.B. Huntington, The Elastic Constants of Crystals, in: London, Edinburgh, Dublin Philos. Mag. J. Sci., 1958: pp. 213–351. doi:10.1016/S0081-1947(08)60553-6.

FIGURES

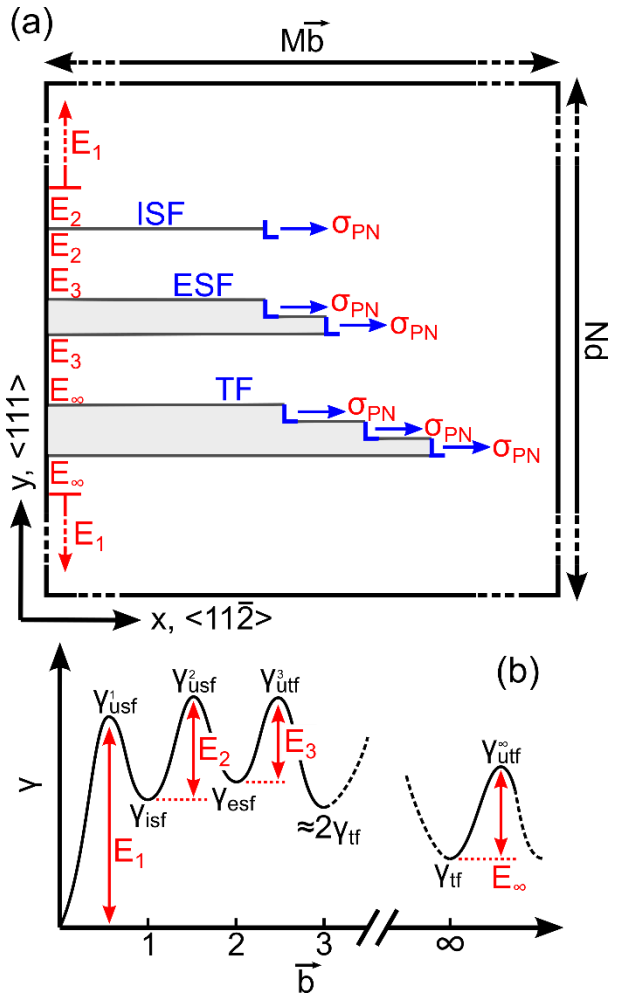

Figure 1: (a) The cell construction considered in kMC simulations. The relevant crystal directions and geometric parameters are indicated. Examples of twin fault structures are depicted schematically. The process barriers are indicated, as determined by the local defect environment. (b) The GSF landscape along the $< 11\bar{2} >$ crystal direction. The relevant GSF energies for the nucleation and growth of a twin embryo from Shockley partial dislocations are indicated. The values along the abscissa indicate the number of leading partial dislocations required to create each structure. The process barriers are defined graphically. See main text for further details.

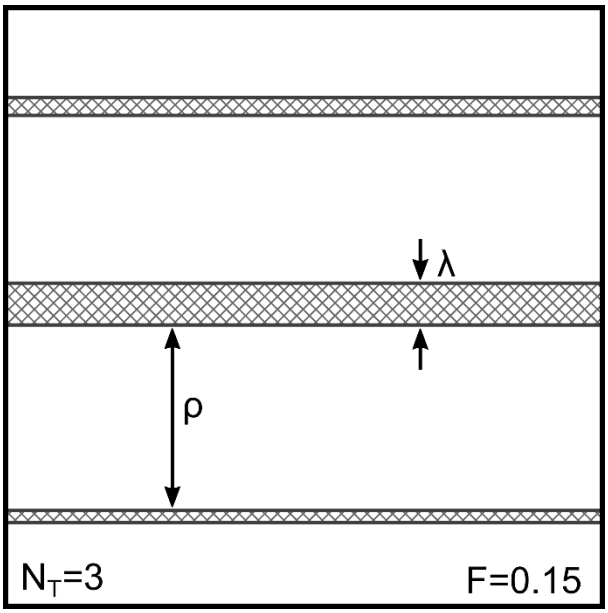

Figure 2: A schematic of a kMC simulation cell that is segmented by 3 deformation twins of varying thicknesses at a twin fraction of 0.15. The twin thickness (λ) and free path (ρ) are indicated.

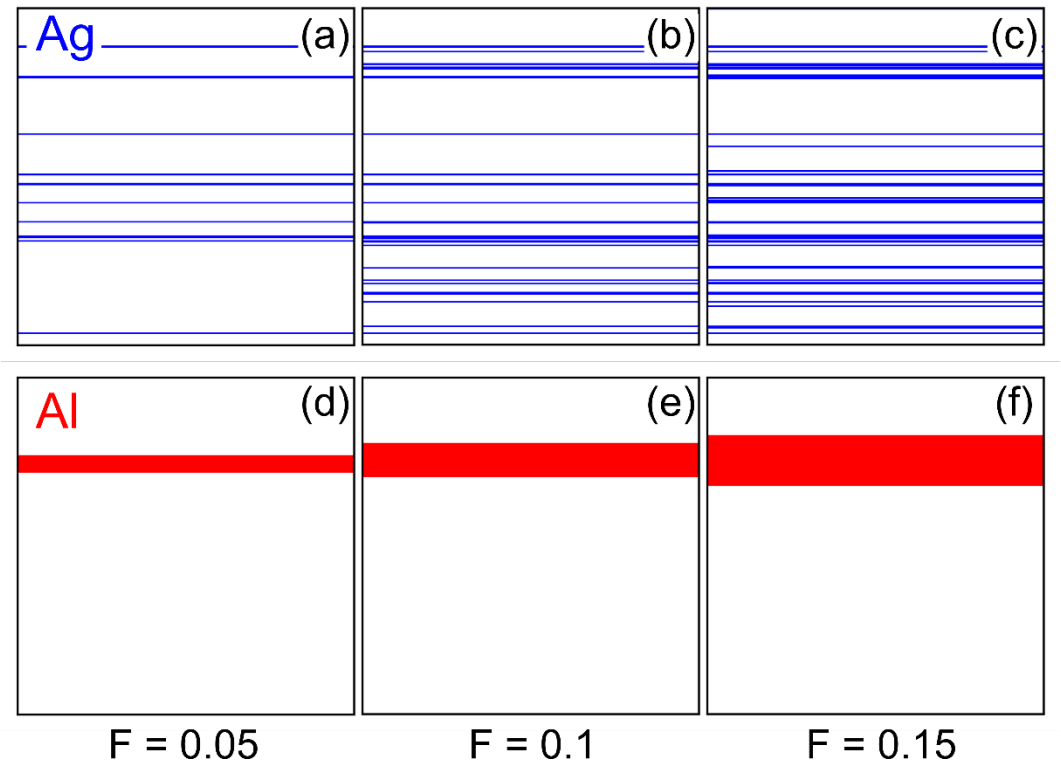

Figure 3: (a)-(c) kMC snapshots for deformation twinning in Ag at twin fractions of 0.05, 0.1, and 0.15. The simulation cell is segmented by a number of deformation twins. (d)-(f) By contrast, Al nucleates a single deformation twin, which continually thickens upon subsequent increases of *F*.

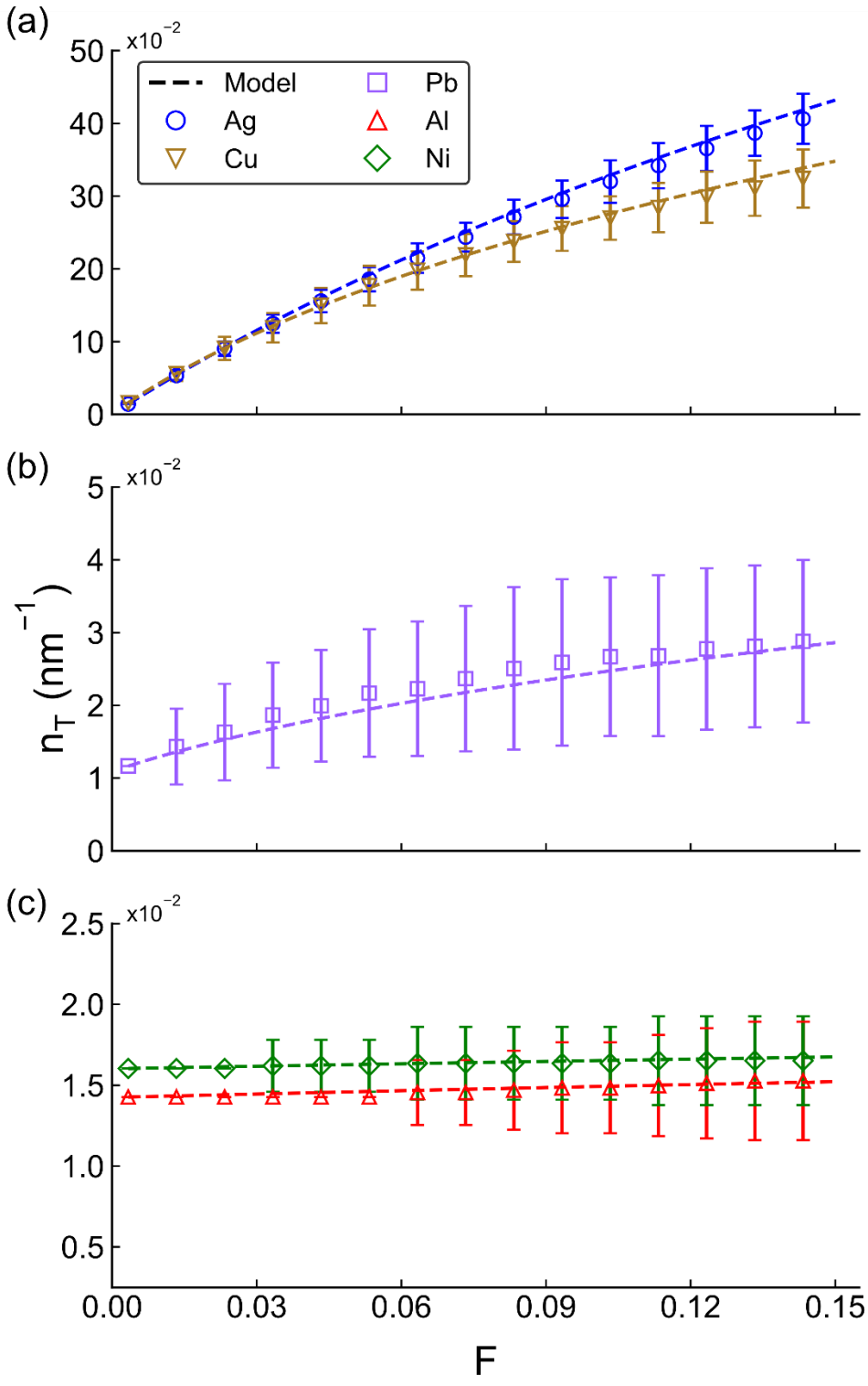

Figure 4: The evolution of the twin number density as predicted by kMC simulations. The data is plotted for Ag and Cu (a), Pb (b), and Al and Ni (c). Calculations from the analytical model are overlaid for each material. Error bars represent ± 1 standard deviation over 100 replications of the kMC simulation.

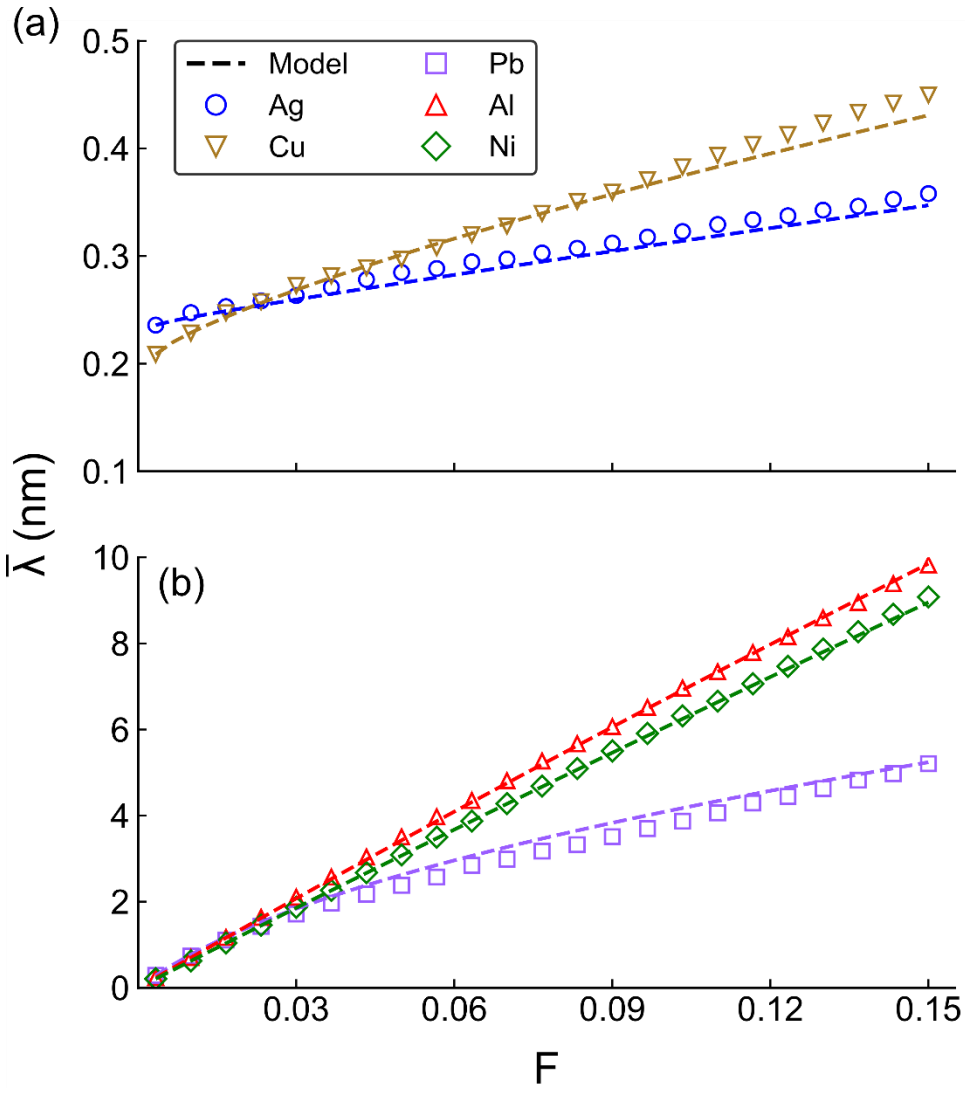

Figure 5: kMC predictions for the evolution of the average twin thickness. Results for Ag and Cu are plotted in (a) and Pb, Al, and Ni are plotted in (b). The analytical predictions are overlaid for each material.

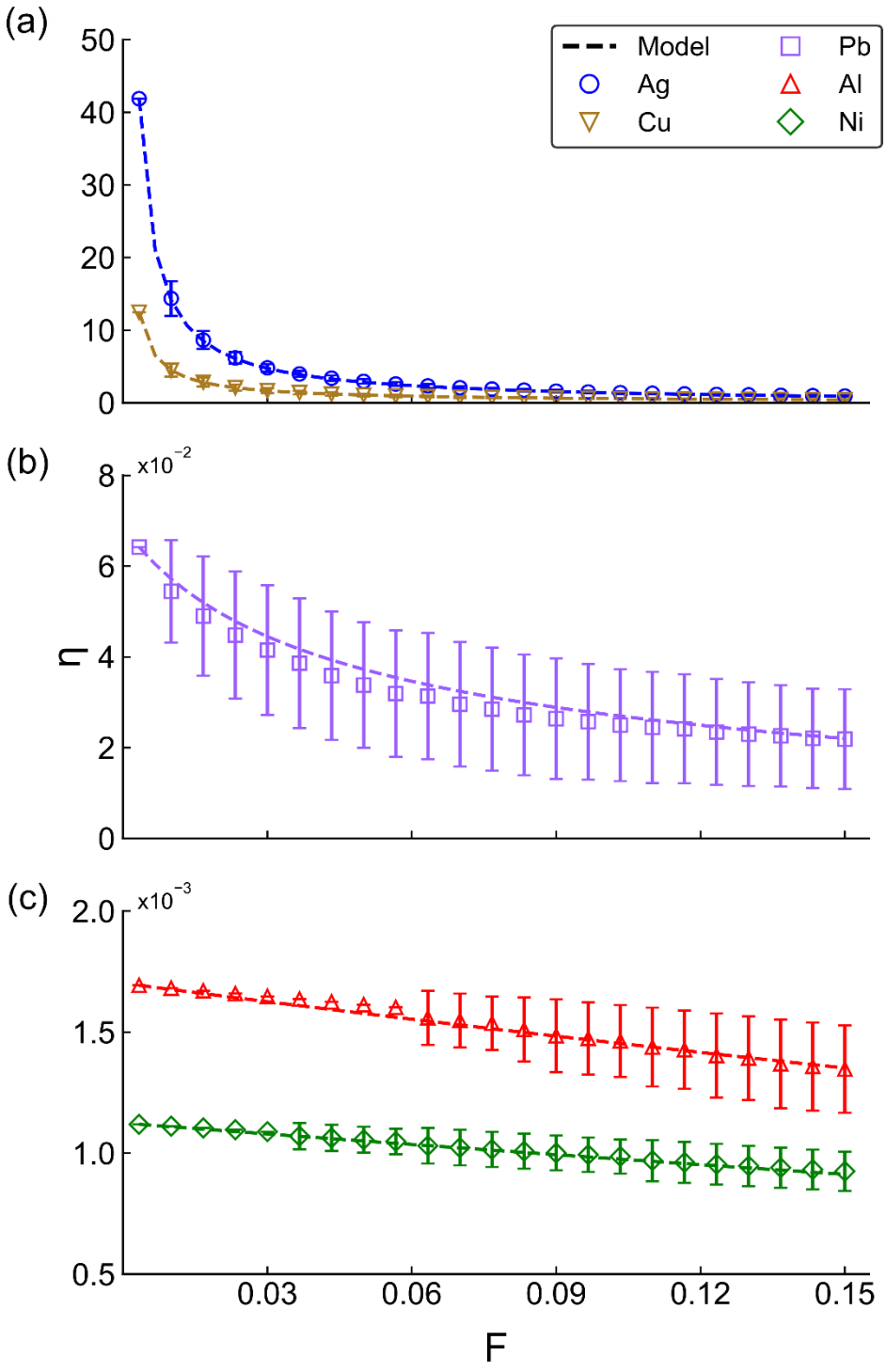

Figure 6: kMC predictions for the evolution of the twin nucleation tendency parameter for Ag and Cu (a), Pb (b), and Al and Ni (c). The analytical model predictions are provided for each material. Error bars represent ± 1 standard deviation over 100 replications of the kMC simulation.

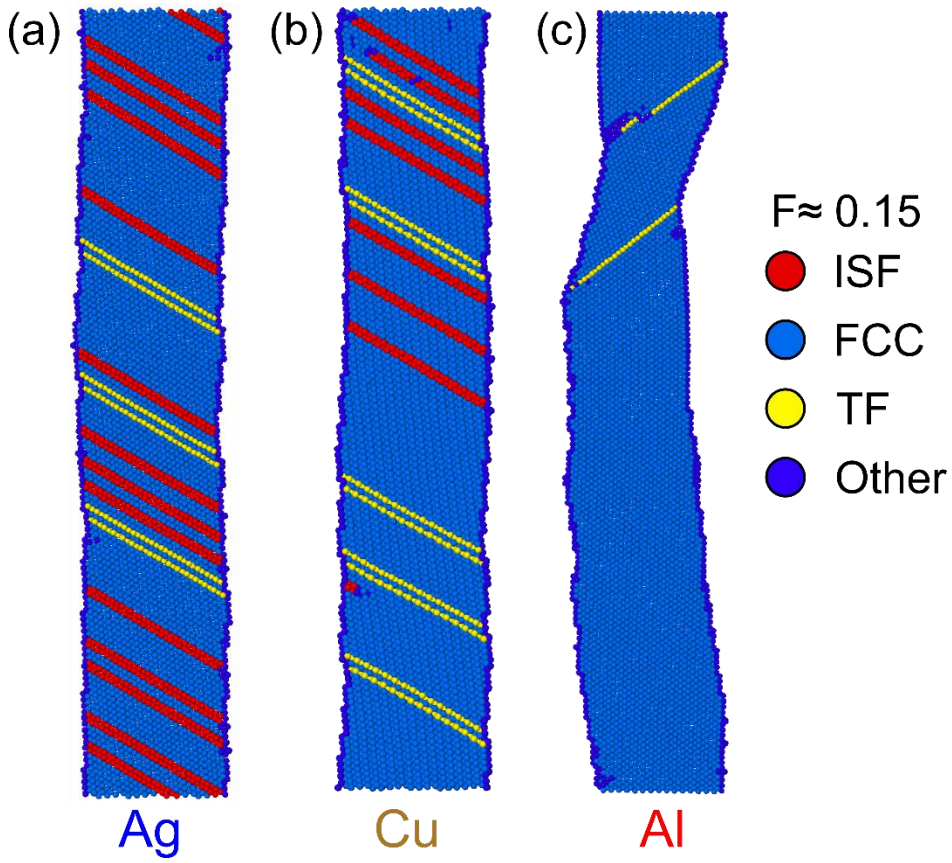

Figure 7: Snapshots of the deformed nanowire topologies from MD tensile simulations at a twin fraction of ≈ 0.15. Snapshots are presented for Ag (a), Cu (b), and Al (c). Red and yellow coloring represent atoms at an ISF or a TF, respectively. ESFs are colored here as TFs. Atoms with an FCC coordination are in light blue and atoms with an unspecified configuration are in navy.

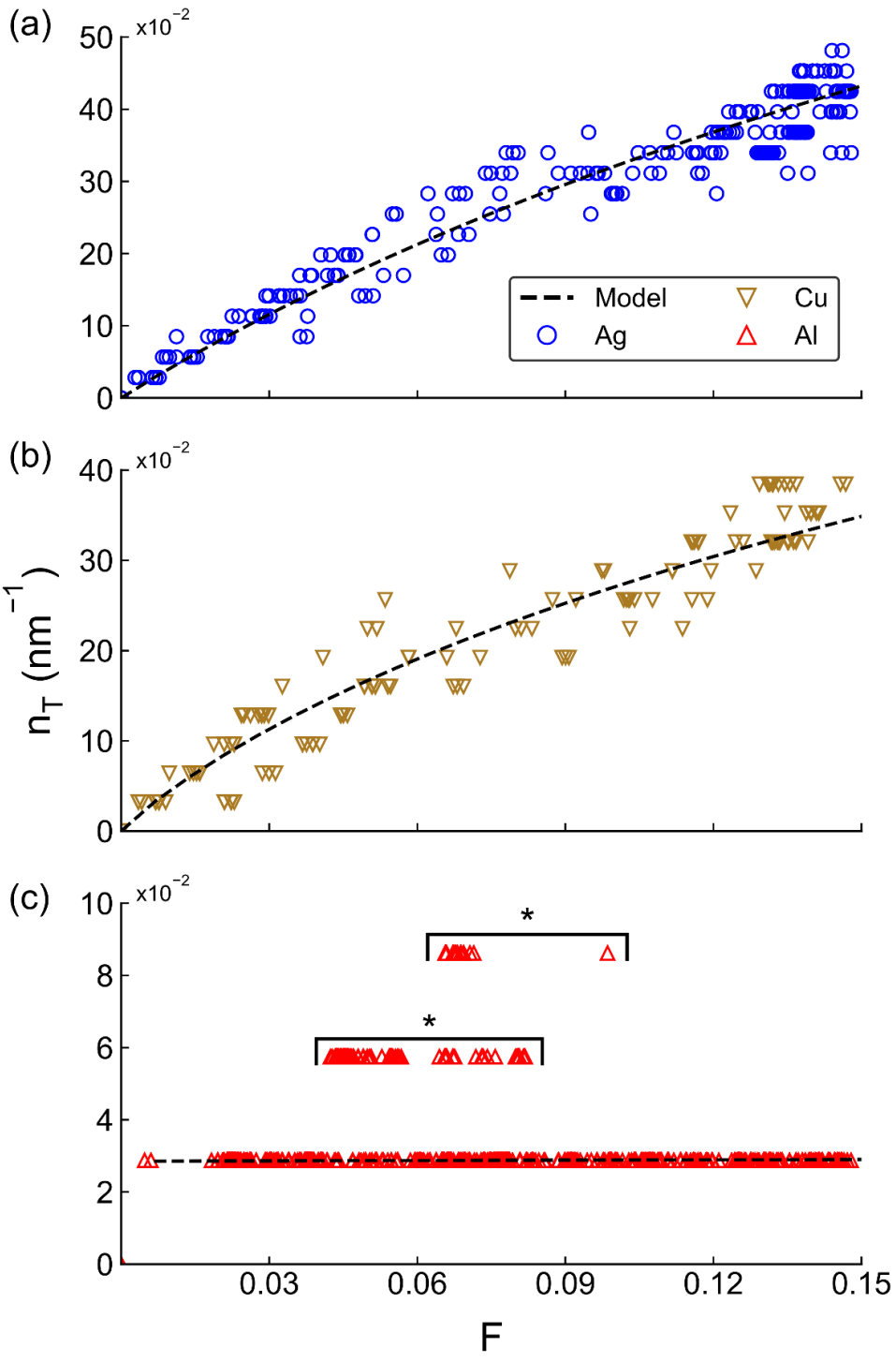

Figure 8: The twin number density evolution as measured in nanowire MD simulations. Five replications were performed for Ag (a), Cu (b), and Al (c). All datapoints from each replication have been plotted. Artifacts associated with isolated incidences of dislocation slip are indicated with an asterisk. The predictions of the analytical model for a nanowire of the same dimensions are plotted in black stroke for each material.

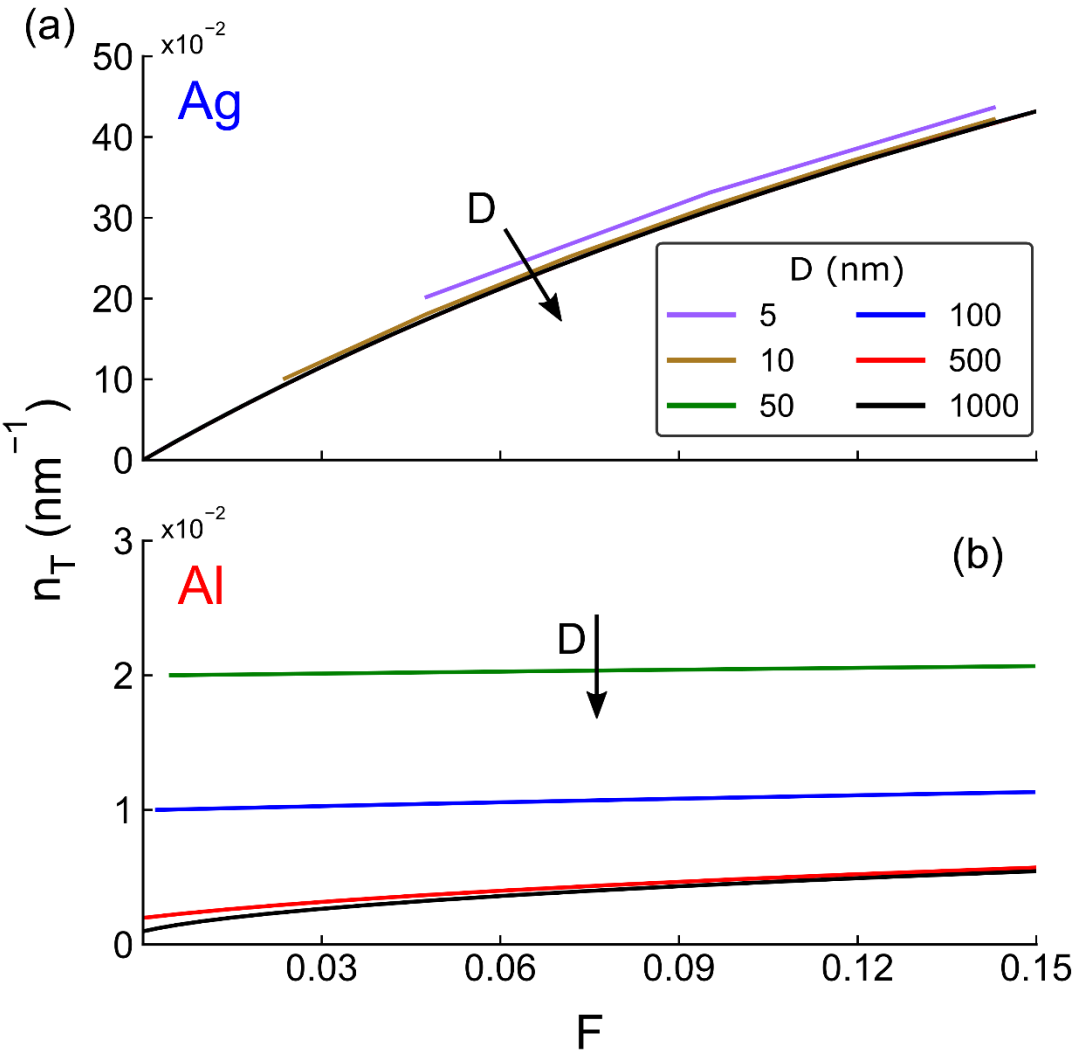

Figure 9: The twin number density evolution at crystal sizes measuring between 5 and 1000 nm. Results are plotted for Ag (a) and Al (b). n_T is observed to converge for Ag at small crystal sizes, whereas it does not approach saturation for Al until $D > 500$ nm.

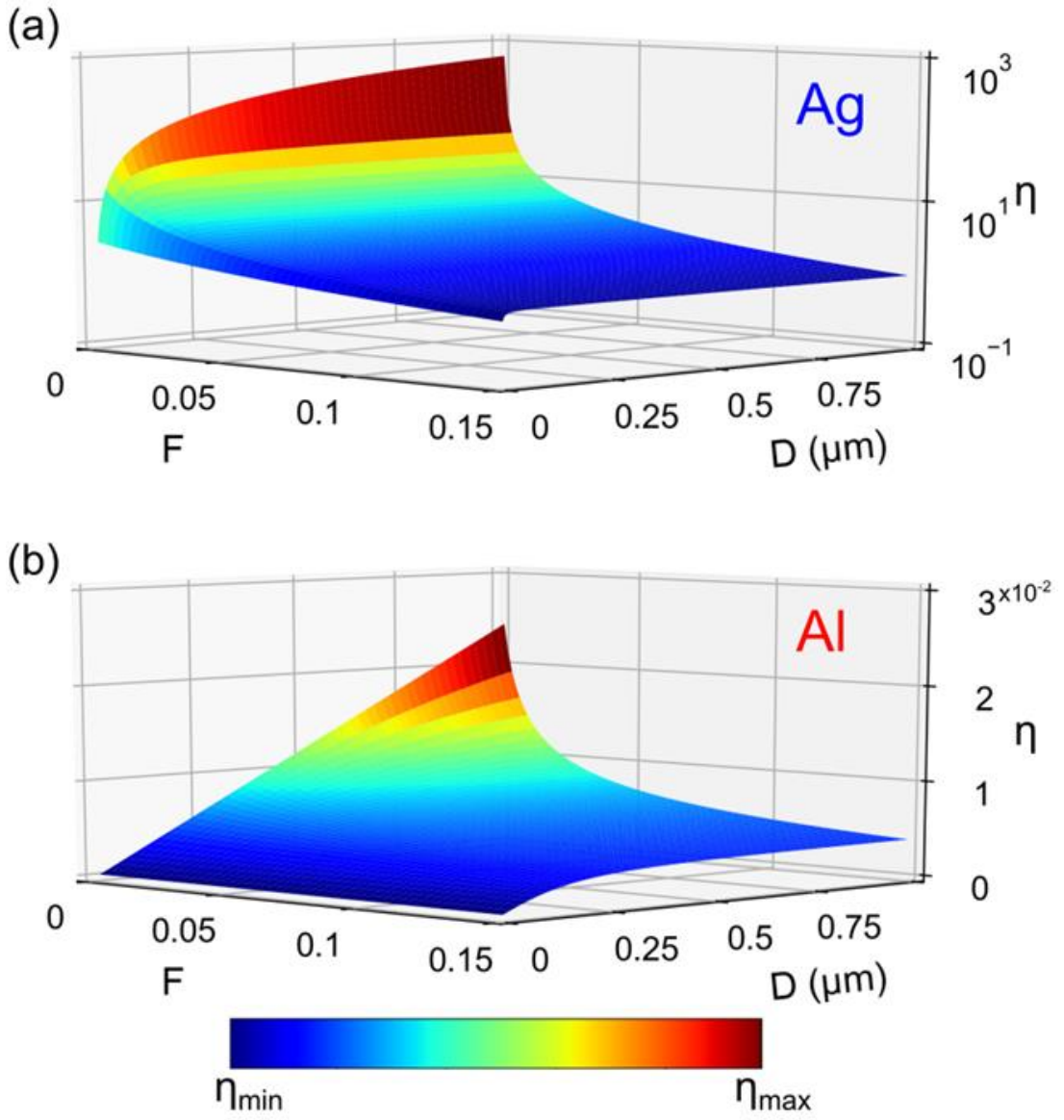

Figure 10: Surface plots of analytical predictions for the twin nucleation tendency. Results are plotted for Ag (a) and Al (b) at twin fractions ranging from 0 to 0.15 and crystal sizes from 5 – 1000 nm. Ag data is plotted on a logarithmic scale. The colormap extremes represent the minimum and maximum values of η for each subfigure.

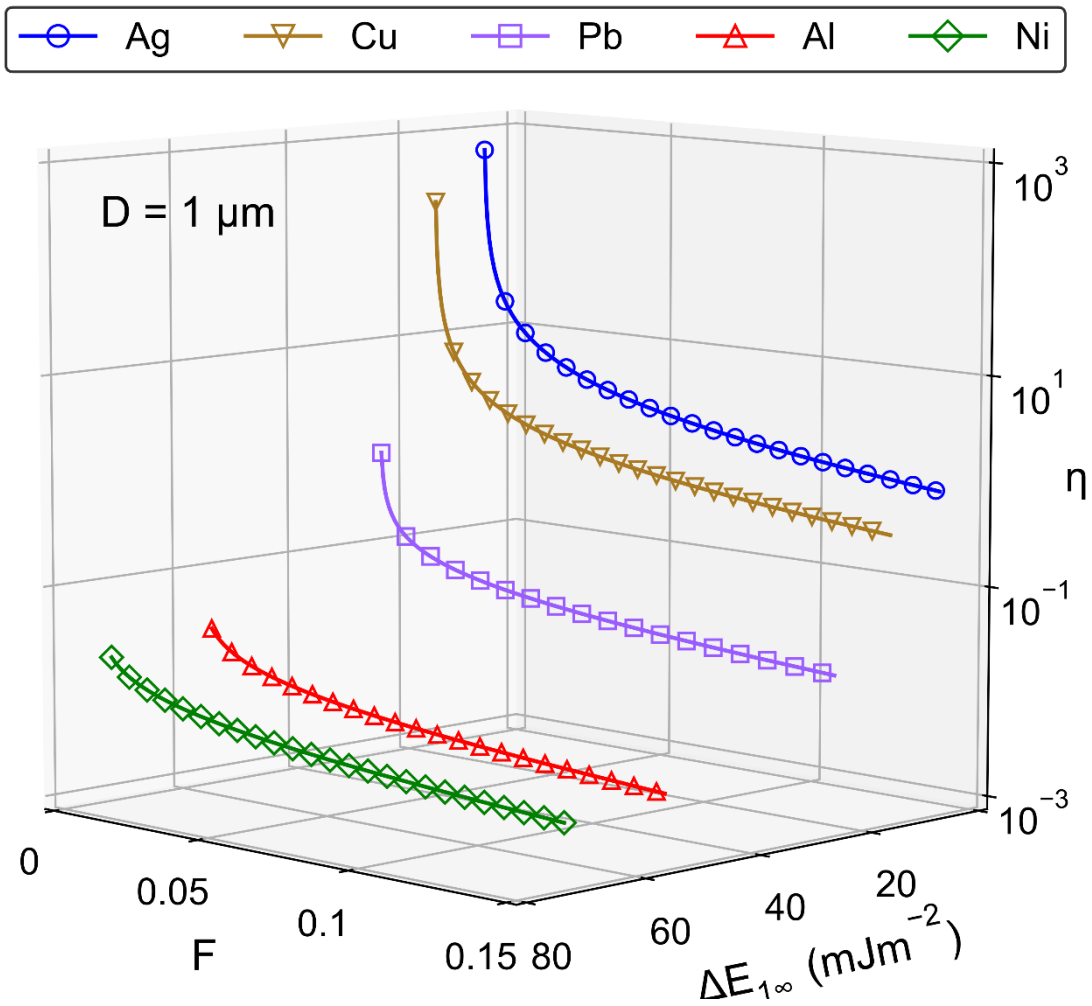

Figure 11: A plot of the twin nucleation tendency of each FCC material examined in this study. These results are plotted against twin fraction and the process barrier difference for a crystal size of $D = 1$ μm.

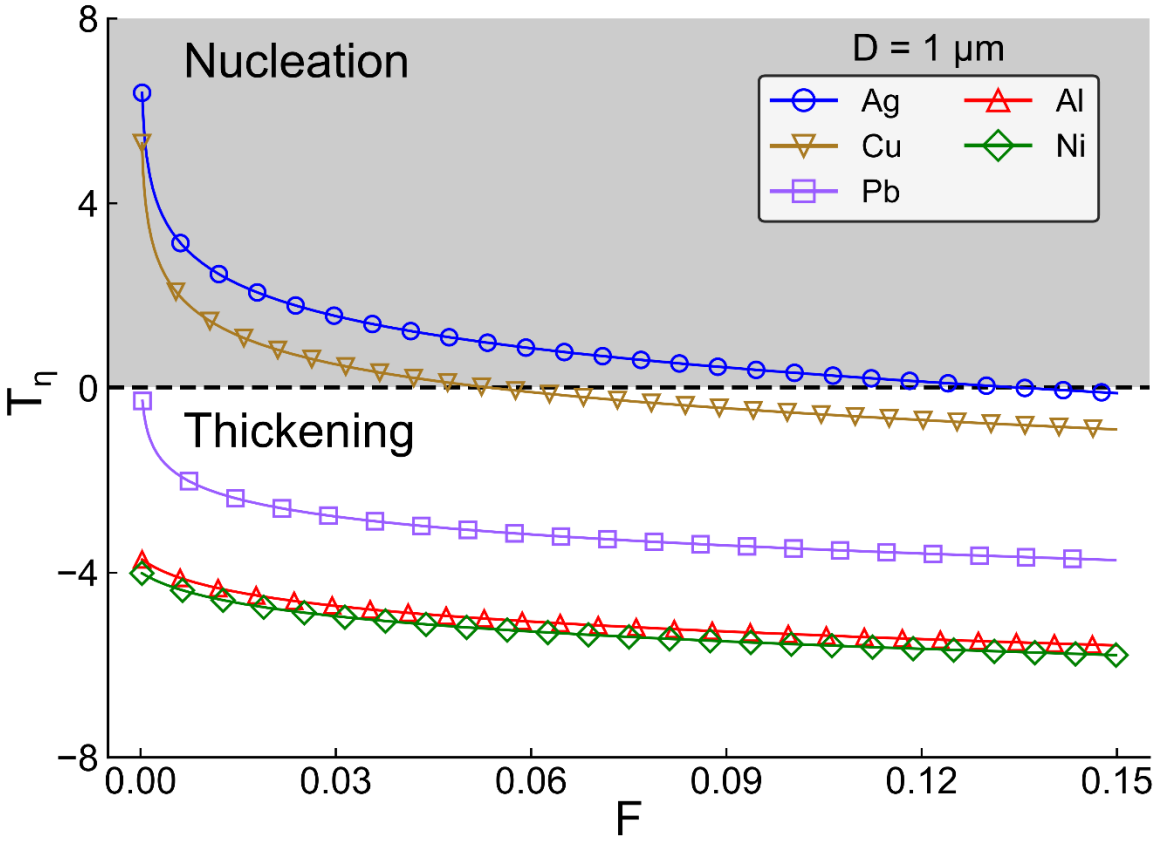

Figure 12: Evolution of the twin nucleation tendency criterion for each of the FCC metals examined in this study ($D = 1$ μm). Nucleation-favored deformation is predicted when $T_\eta > 0$ and thickening-favored twinning is expected when $T_\eta < 0$. Ag and Cu are predicted to favor twin nucleation – particularly at low values of F. Pb, Al, and Ni exhibit a preference for thickening-favored twinning. However, as the twin fraction increases, each material exhibits a monotonic decrease in T_η as sites for new twin nucleation become progressively occupied by faults. Ag and Cu crossover into thickening-favored deformation at twin fractions of ≈ 0.14 and 0.06, respectively.

TABLES

Table 1: Twinnability criteria used to predict tendency for dislocation slip or deformation twinning. GSF energies for each criterion have been formatted using the notation implemented in this study (see Figure 1).

Twinnability criterion	Deformation modes	Criterion ranges	Ref.
$T_{TB} = \left(1.136 - 0.152\frac{\gamma_{isf}}{\gamma^1_{usf}}\right)\sqrt{\frac{\gamma^1_{usf}}{\gamma^2_{usf}}}$	dislocation slip, twinning	T_{TB} < 1.1, slip favored T_{TB} ≥ 1.1, twinning favored	[2,7]
$T_{AS} = \sqrt{3\frac{\gamma^1_{usf}}{\gamma^2_{usf}} - 2\frac{\gamma_{isf}}{\gamma^2_{usf}}}$	dislocation slip, twinning	T_{AS} < 1, slip favored T_{AS} ≥ 1, twinning favored	[4,7]
$T_{Jin} = \frac{\gamma_{isf}}{\gamma^1_{usf}}$	dislocation slip, twinning	T_{Jin} ≤ 0.8, twinning favored T_{Jin} > 0.8, slip favored	[5,7]
$T_{Jo} = \frac{\gamma_{isf}}{\gamma^1_{usf} - \gamma_{isf}}$	dislocation slip, twinning, stacking fault emission	T_{Jo} ≤ 0, stacking fault favored[a] 0 < T_{Jo} < 2, twinning favored[a] T_{Jo} ≥ 2, slip favored[a]	[6,7]

[a]T_{Jo} also considers the applied shear direction in its formulation. Values stated here are for shear directed along the <112> twinning direction.

Table 2: Material parameters, Debye frequencies, and GSF energies[a] $\left(\frac{mJ}{m^2}\right)$, used in kMC simulations.

Material	$\vec{b}$ (nm)	d (nm)	G (GPa)[b]	ν[b]	R_o (10^{13}/s)	γ^1_{usf}	γ^2_{usf}	γ^∞_{utf}	γ_{isf}	γ_{esf}	γ_{tf}
Ag	0.167	0.236	25.5	0.39	3.94	91	100	93	16	12	8
Al	0.165	0.234	26.2	0.35	9.66	140	196	135	112	112	50
Cu	0.148	0.209	40.0	0.37	7.98	158	179	161	36	40	18
Ni	0.147	0.208	77.7	0.31	9.88	258	323	251	133	138	65
Pb	0.202	0.286	6.7	0.42	2.70	55	79	53	48	48	23

[a]From Ref. [5]
[b]Calculated from compliance constants in Ref. [56] using a Reuss averaging assumption.

Table 3: Comparison of criteria versus the initial calculated twin nucleation tendency for a crystal with D = 1 μm. The criterion derived in this study (T_η) is compared against those of Tadmor and Bernstein [2] (T_{TB}), Asaro and Suresh [4] (T_{AS}), Jin *et al*. [5] (T_{Jin}), and Jo *et al.* [6] (T_{Jo}).

		Criterion				
Material	η_1	T_η	T_{TB}	T_{AS}	T_{Jin}	T_{Jo}
Ag	597.4	6.39	1.06	1.55	0.18	0.21
Cu	200.9	5.30	1.03	1.50	0.23	0.30
Pb	0.756	-0.28	0.84	0.93	0.87	6.86
Al	0.024	-3.71	0.86	1.00	0.80	4.00
Ni	0.018	-4.06	0.95	1.25	0.52	1.06